



Cite this: *Soft Matter*, 2019, 15, 2817

Magnetically stimulating capillary effect for reversible wet adhesions†

Meng Li, Qingwen Dai, Qing Jiao, Wei Huang  and Xiaolei Wang *

Despite fascinating natural examples of switchable adhesives to wet surfaces, strategies for an artificially switching capillary adhesion system *in situ* remains a challenge. Here, we develop a smart reversible magnetic fluid (MF) meniscus adhesion system whose capillary effect can be regulated by external magnetic stimuli. It is revealed that the MF filled joint between two solid surfaces undergoes alteration of its adhesive properties in response to the external stimulus of a varying magnetic field. Compared with the original capillary force (without stimuli), the stimulated one increases or decreases depending on the distributions of applied magnetic field intensities, allowing for switchable adhesive behavior. In addition to the Laplace pressure, hydrostatic pressure induced by the intensity difference in the magnetic field between the inner and outer surfaces of the meniscus was found to contribute to wet adhesion, which accounted for the reversibility. Theoretical models of reversible adhesions have been built and solved as well, and agree well with the experiment results. Our findings not only provide a deep understanding of MF capillary adhesion, but also provide a new method to design reversible wet adhesion systems.

Received 7th February 2019,
Accepted 7th March 2019

DOI: 10.1039/c9sm00270g

rsc.li/soft-matter-journal

1. Introduction

Reversible interfacial adhesives possessing an alterable strength through the modification of near-surface architecture or surface chemistry attract much attention for their large potential in practical applications in industry or daily life. Fascinating examples are widely found in natural organisms, such as the well-known hairy feet of geckos, allowing free dynamic alteration of adhesion to dry surfaces *via* the orientation and compliance of the fibrillar topography.^{1–4} Inspired by this dry adhesion, diverse artificial fibrillar surfaces characterized with reversible regimes have been developed. The main approach for regulation is utilizing surface topography reorganization *via* the application of an external physical stimulus, such as temperature,^{5–7} magnet,^{8,9} or preload.^{10–12}

Another type of celebrated biological model is switching interfacial adhesives under wet conditions, which is usually found on tree frogs, torrent frogs, and newts.^{13–18} Unlike the gecko, these amphibians are capable of securing their unrestrained locomotion to wet substrates without slipping or falling off using their adhesive toe pads patterned with a polygonal microstructure of epidermal cells separated by narrow mucus-filled channels.^{19–21}

The underlying mechanisms were generally suggested to be contributions from capillary forces, frictional forces, and viscous forces to the wet attachment,^{20,22} distinct from the protein adhesive of mussels.²³ Although recent studies effectively demonstrated the positive role of high friction induced by toe-pad topographies for wet climbing,^{19,24–26} the shear force seems to be irrelevant for switching or reversing. This is because the normal adhesive interaction of amphibians with wet surfaces is mainly based on capillary forces induced by the visible meniscus around the toe pads, especially under the mode of standing upright or hanging upside down.^{20,27} These amphibians seem to have evolved a perfect organic system that can dynamically tune capillary forces to achieve a switchable attachment to wet substrates. Some background mechanisms based on dynamic actuation of the epidermis's topography or amount of liquid meniscus have also been hypothesized.^{28,29} The mechanism of the chemical modification of the toe pads' secretion to regulate capillary forces for reversible adhesion is still unclear.²²

Despite exciting progress in studying the toe pads for wet attachments, strategies to artificially tune the capillary effect for reversible adhesion to wet surfaces are scarce because of the complex interfacial interaction, so this mechanism remains a challenge. Previous studies indicated that the capillary strength of solid–liquid–solid systems are generally dominated by the interfacial adhesive property of the middle meniscus with solids, which suffers from the influence of solid geometries,^{30–32} environmental conditions,^{33–35} materials,^{36,37} *etc.* Some approaches, such

National Key Laboratory of Science and Technology on Helicopter Transmission, Nanjing University of Aeronautics & Astronautics, Nanjing 210016, China.
E-mail: wxl@nuaa.edu.cn; Fax: +86-25-84893630; Tel: +86-25-84893630

† Electronic supplementary information (ESI) available. See DOI: 10.1039/c9sm00270g

as changing probe shape,^{38–40} splitting wedged film,⁴¹ modifying surface chemicals^{42,43} and structures,⁴⁴ or employing contact-angle hysteresis,^{45–47} have been also developed experimentally or theoretically to permanently alter the adhesive performance of the capillary meniscus. However, compared with the artificial reversibility of dry adhesion, these methods to regulate capillary adhesion are cumbersome and irreversible, and most importantly, it is difficult for them to enable a timely response of adhesive switching *in situ*.

Herein, we report a facile strategy that exploits the external magnetic field to stimulate the capillary force to achieve reversible or controllable wet-adhesion systems. In this work, a functional liquid, magnetic fluid (MF), was employed to produce the meniscus between the spherical probe and substrate, and the external stimuli of varying magnetic fields were simulated by applying coin-shaped permanent-magnets with various diameters. We systematically studied the effect of the varying distribution of an external magnetic field on the capillary adhesion strength of the probe–MF–glass system, and revealed the mechanism underlying the switching role. The relative theoretical models were also built and solved for comparison with the experimental results. To the best of our knowledge, this is the first example of achieving a reversible or controllable wet-adhesion system *via* magnetically tuning the capillary effect.

2. Material and methods

2.1 Capillary meniscus and magnetic field

MFs are formed by single-domain magnetic nanoparticles dispersed in a carrier liquid, which are usually used for industrial tribology and sealing. Here, Fe₃O₄-based MFs (SS-F10A2; saturation magnetization M_s of ~ 100 Gs, density ρ of ~ 0.89 ; surface tension γ of ~ 23.8 mN m⁻¹ at 25 °C) prepared by the co-precipitation technique were used to produce the liquid bridge between the probe and glass substrate. The varying stimuli of external magnetic fields were achieved using coin-shaped magnets (N35 NdFeB) with various diameters (ESI,† Fig. S1a), which stick to the back of the glass substrate. The height of the magnet is fixed at 2 mm, and the diameter d ranges from 2 mm to 9 mm.

Adhesion measurements. Adhesion measurements were performed using a custom-made setup, as shown in Fig. 1a, which was detailed in ref. 48 The SiO₂ substrate (1 mm in thickness) with a magnet fixed on the center of the back was placed on a mobile stage, and the glass probe (18.5 mm in curve radius, R) was mounted at the end of a cantilever with a small mirror. The wet-adhesion test process is briefly described as follows: first, a small MF drop was placed on the glass sheet using a micropipette (ESI,† Fig. S1b and c), and then the drop was positioned at the center of the SiO₂ probe by moving the stage under the microscope monitor. The probe was then

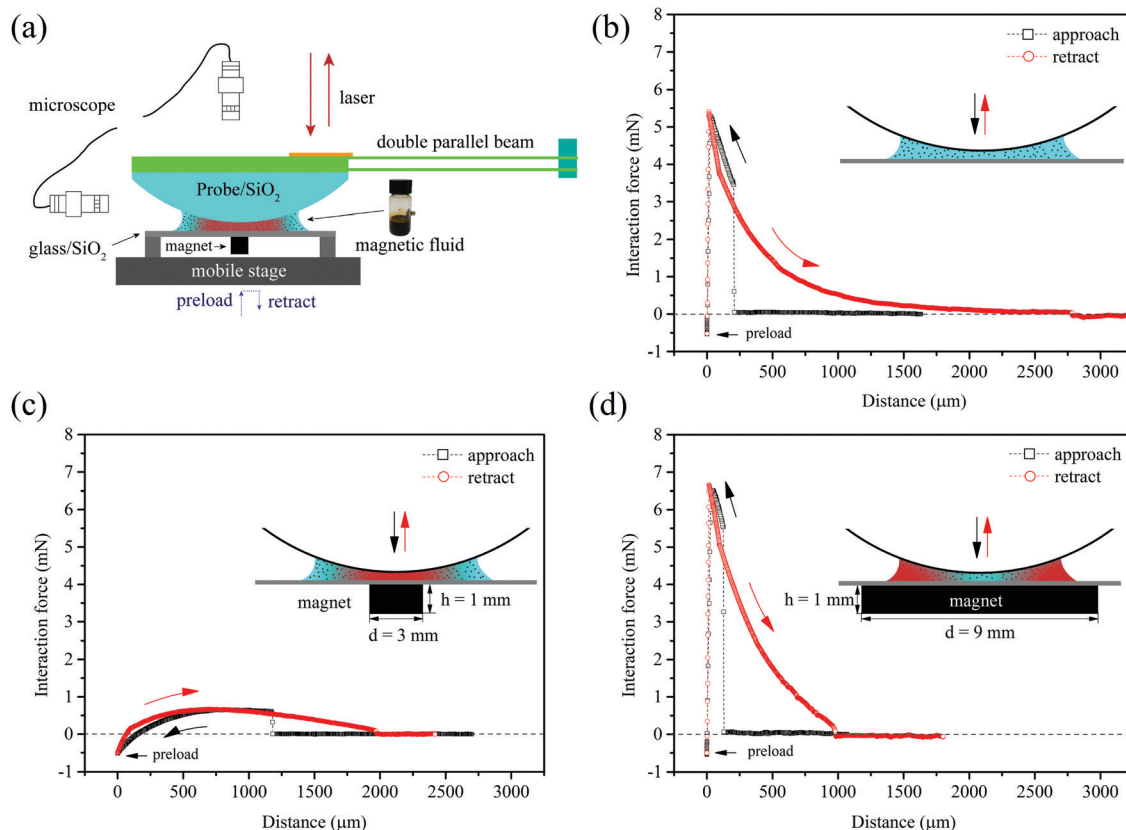


Fig. 1 (a) Experimental setup for measuring wet adhesion forces. (b) Force–distance curves of capillary bridge of MF between the probe and glass substrate, (c) with the magnet of $d = 3$ mm, (d) with the magnet of $d = 9$ mm. The black and red lines indicate the probe approaching and retracting, respectively.

pressed into the drops to contact the glass substrate with a preload of 0.5 mN. After a holding time of 5 s, the mobile stage retracted at a speed of $10 \mu\text{m s}^{-1}$ to break the capillary interaction of the liquid meniscus. Throughout the entirety of the above process, the force interaction between the probe and substrate was measured using a laser interferometer and recorded on the computer. Each test was performed at least five times.

3. Results and discussion

3.1 Switched capillary force of MF meniscus for reversible adhesion using magnetic stimuli

Fig. 1b–d show the representative force–distance curves of the $5 \mu\text{L}$ MF meniscus measured between the probe and substrate with and without magnetic stimuli. The black lines indicate the force interaction during the probe's approach for loading, and the red lines represent the probe retracting for unloading. When measuring the adhesion force of the MF meniscus in the absence of a magnetic field, the force–distance curves (Fig. 1b) behave smoothly with a long distance of approximately $2750 \mu\text{m}$, yielding the highest force of approximately 5.4 mN (original capillary force). The applied magnetic field led to a pronounced influence on the capillary interaction of the MF

meniscus, both in the force value and interacted distance. For a coin-shaped magnet of $d = 3 \text{ mm}$, the capillary force of the MF meniscus decreased significantly, only showing a value of approximately 0.668 mN (Fig. 1c), and the interaction distance also decreased to approximately $1900 \mu\text{m}$. However, for the coin-shaped magnet with a large diameter of $d = 9 \text{ mm}$ (Fig. 1d), the capillary force of the MF meniscus surprisingly increased to a value of approximately 7 mN, even surpassing the original capillary force (Fig. 1b), while the interacted distance continued to decrease. It appears that the capillary interaction of the MF meniscus between two surfaces can be regulated by the external magnetic stimuli, and with a well-designed magnetic field, switchable and controllable wet adhesion is artificially possible.

3.2 Influence of magnet diameter and liquid volume on the capillary interaction of MF meniscus

Fig. 2a shows the side views of MF meniscus (fixed at $5 \mu\text{L}$) between the probe and substrate with/without a magnetic field ($d = 2, 9 \text{ mm}$) captured under the microscope system. β is the filling angle of the meniscus and L is the filling radius. It can be seen clearly that for a constant volume of meniscus, the contact area between the MF meniscus and substrate changes slightly between the experiments with and without magnetic stimuli. Fig. 2b shows the actual filling radius L and filling angle β of

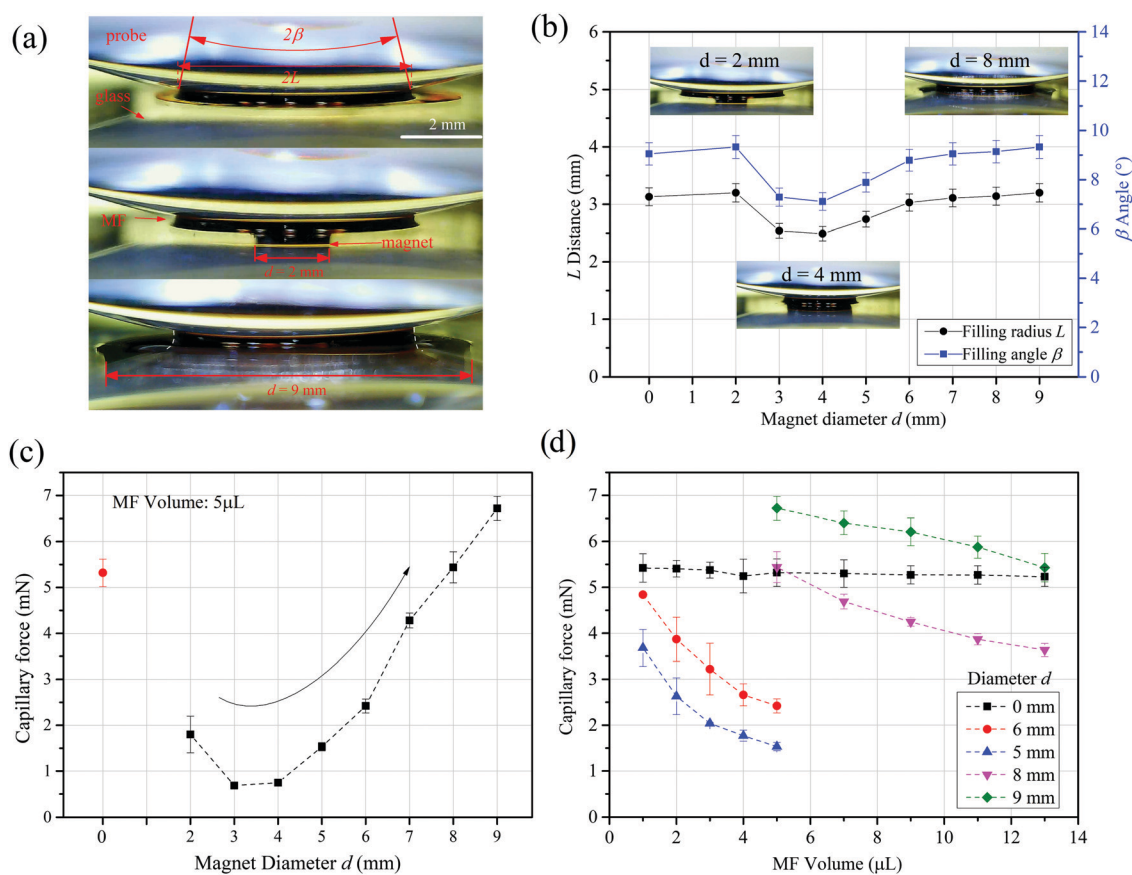


Fig. 2 (a) Side views of the MF meniscus between probe and glass substrate with and without the magnetic stimuli. (b) Filling radius L and filling angle β of MF meniscus measured with the stimuli of magnets with varying d ($d = 0$ indicates the case without magnetic stimuli). (c) Capillary forces of the MF meniscus measured with magnetic stimuli of varying d . (d) Capillary forces of MF meniscus as functions of liquid volume with/without magnetic stimuli.

the MF meniscus (fixed at $5\ \mu\text{L}$) measured with the stimulus of a magnet with varying d ($d = 0$ indicates the case without magnetic stimulus) using the microscope. Both L and β decreased at first, and then increased with increasing d of the magnet, exhibiting the lowest value at $d = 4$ mm. This means that the coin-shaped magnet of $d = 4$ mm may have the strongest magnetic field, which firmly adsorbs the MF drop with little spreading under the indentation of the probe. For a constant volume, the lowest L or β also signifies the thickest film of MF between the probe and glass substrate.

The normal capillary forces for wet adhesion stimulated by magnets with varying d are shown in Fig. 2c. As can be seen, the original capillary force of the MF meniscus between the probe and substrate is approximately 5.32 mN, and the external magnetic stimuli for adhesion shows dependence on diameter. Compared with the original capillary adhesion, the capillary force of the MF meniscus stimulated with the magnet of $d = 2$ mm decreased to 1.8 mN, and as d increases, the capillary force first decreases, then increases. $d = 3$ mm achieved the lowest force value of approximately 0.68 mN, and $d = 9$ mm achieved the highest value of approximately 6.8 mN, exceeding the original capillary force. Fig. 2d shows the capillary forces of the MF meniscus as functions of liquid volume with/without the magnetic stimuli. The capillary force measured without magnetic stimuli did not vary significantly with MF volume. In contrast, for the magnetic stimuli of $d = 5, 6, 8,$ and 9 mm, the capillary forces decreased obviously with the increase in MF volume. In summary, our results suggest that the capillary force of the MF meniscus can be regulated by the external magnetic field, and the coin-shaped magnet diameter and volume of the MF both have an influence on the strength of the stimulated capillary interaction.

3.3 Why the magnetic field alters the capillary force of the MF meniscus and how to design magnetic stimuli for controllable wet adhesion

The results of the adhesion tests in the previous sections demonstrated that the external magnetic stimuli regulated the capillary adhesion of the MF meniscus depending on the diameter of the coin-shaped magnet, and the stimulated capillary forces are very sensitive to variations in volume. The diameter dependence suggested that the distribution of the magnetic field intensities may account for the effect of magnetic stimuli on capillary adhesion. Moreover, we can also attribute the increasing stimulated capillary force with increasing meniscus volume to the influence of the magnetic field distribution for the following reason. From previous capillary theory,³² the normal force of the sphere-liquid-flat system increases with the increased liquid volume; however, it can be neglected here because of the very small range of volume variation. This was confirmed by the negligible change in capillary force with the increased volume in the absence of magnetic stimuli (Fig. 2d).

To reveal the mechanism for tunable capillary force of the MF meniscus, the distributions of the field intensities for all magnetic stimuli (d varying from 2 to 9 mm) were calculated by

using finite-element simulation software (Ansoft Maxwell 14.0). Fig. 3a shows the characteristic contours of field intensities in the half-space above the substrate with $d = 2, 4,$ and 9 mm. The field intensities H of the substrate surface generated by magnets with various d are displayed as a function of position in Fig. 3b. It can be found that the peak magnetic field intensity for $d = 2$ mm is at the center of the substrate, giving approximately $113\ \text{kA m}^{-1}$, and with increasing d , this peak value increased and achieved the highest at $d = 5$ mm, then the peak

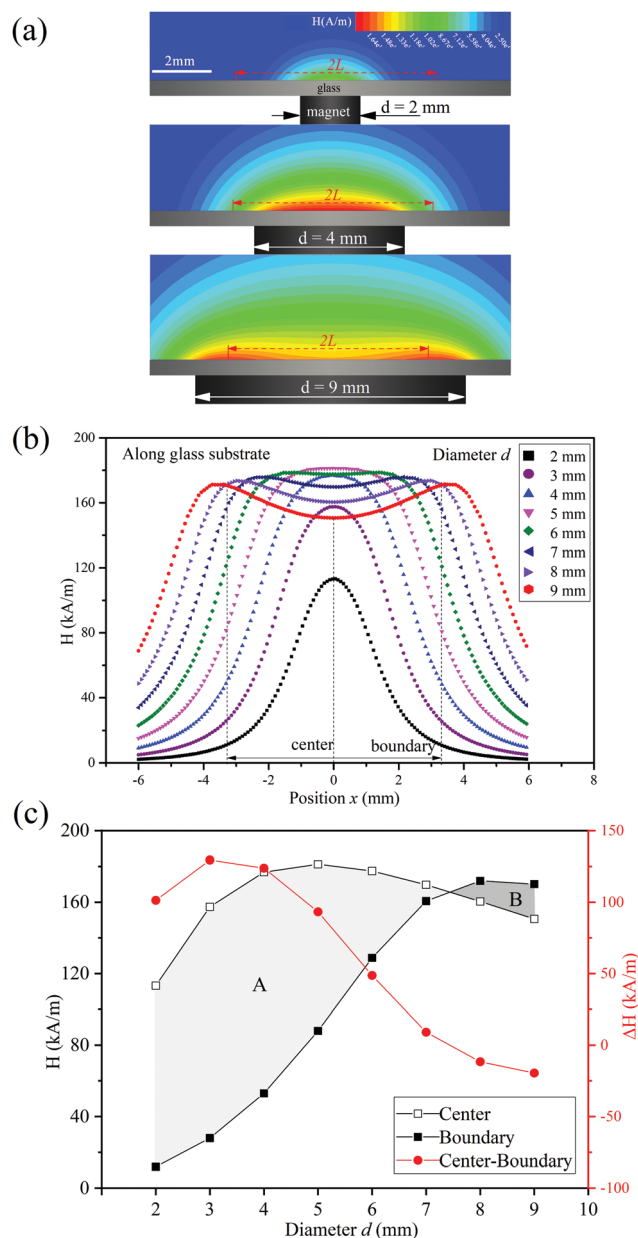


Fig. 3 (a) Contours of magnetic field intensities for the magnets of $d = 2, 4,$ and 9 mm in the half-space above substrate. (b) Magnetic field intensities on substrate surface as a function of position with varying d . (c) Magnetic field intensities as a function of d at the center of substrate and the triple-phase boundary of substrate/MF/gas. For ease of comparison, the boundaries for all stimulated menisci were approximately fixed at $x = 3.2$ mm.

of intensity–position curve moves outside across the substrate, creating a valley around the center of the substrate (also reflected in the MF distribution of ESI,† Fig. S1b). As a result, these differences in magnetic fields were suggested to be responsible for the varying capillary force of the stimulated MF meniscus.

Previous studies have demonstrated that the external non-uniform magnetic field caused an attraction potential for the MF, which drives the liquid flow to a more intense magnetic field.^{49–51} If such non-uniform magnetic field performs inside the MF, an additional hydrostatic pressure, ΔP_{Mag} , will form easily due to the difference in magnetic field intensity, ΔH ,^{51,52} just like the pressure in water induced by the different heights or depths in a gravitational field. Fig. 3c shows the magnetic field intensities located at the center of the substrate and the triple-phase boundary of substrate/MF/gas with varying d . Note that the boundary can be nearly regarded as the position L because of the very small height of the meniscus (Fig. 2a); for ease of comparison, the boundary, *i.e.*, L , for all magnets was fixed at $x = 3.2$ mm, though changes slightly with d , especially for $d = 3–5$ mm (Fig. 2b). From observation, there are two distinct regions with varying d , marked as A and B. For region A, the magnetic field intensity at the center is larger than that at the boundary, but for region B, the opposite occurs. The intensity differences ($H_{\text{center}} - H_{\text{boundary}}$) in these two regions were also depicted in Fig. 3c (red line), which interestingly presents an inverse tendency to the stimulated capillary forces of the MF meniscus shown in Fig. 2c. These results indicate that the magnetic field intensity difference between the interior of the meniscus and the boundary interface of the MF and gas may play a key factor that gives rise to the tuning effect on the stimulated capillary force.

In fact, the normal capillary adhesion of the liquid meniscus between two substrates is exerted by a combination of the pressure difference between the inner liquid P_{inside} and outer atmosphere P_{a} (the major contribution) and the surface tension force of the liquids. For the MF meniscus without stimuli, *i.e.*, the original capillary interaction, this pressure difference is totally due to the Laplace pressure ΔP_{Lap} induced by the concave meniscus (ESI,† Fig. S2a), which behaves negatively and is distributed uniformly inside the meniscus (Fig. 2b and 3c). Fig. 4 illustrates the mechanism of the external magnetic stimuli regulating the capillary adhesion of MF meniscus

(red signifying high field intensities and blue signifying low ones). For the magnetic stimuli with a small diameter ($d = 2–7$ mm), the field intensity distribution in Fig. 3b indicates the high value inside the MF meniscus and the low value on the boundary interface of the MF and gas, resulting in a positive difference, $H_{\text{inside}} - H_{\text{boundary}} = \Delta H > 0$. This positive ΔH produces a positive pressure difference from the center of the meniscus to boundary interface, *i.e.*, the magnetically induced pressure $\Delta P_{\text{Mag}} > 0$, which weakens the capillary adhesion between the probe and substrate first caused by the negative Laplace pressure (Fig. 1c and 2c). However, if the diameter of the coin-shaped magnet is enough large, the distribution curves of magnetic fields characterize concave heads (Fig. 3b) which result in a negative ΔP_{Mag} because the boundary interface has a more intense magnetic field than the inside of the meniscus, $H_{\text{inside}} - H_{\text{boundary}} = \Delta H < 0$. As a consequence, the negative Laplace pressure ($\Delta P_{\text{Lap}} < 0$) and magnetically induced pressure ($\Delta P_{\text{Mag}} < 0$) both play a positive role for capillary adhesion, leading to a higher adhesion force than the original capillary force (without magnetic stimuli) (Fig. 1 and 2c). For a clear comparison, the above characters of capillary adhesion were expressed using absolute value in Fig. 4, and $|P_{\text{inside}} - P_{\text{a}}|$ reflected the adhesion strength. In addition, the influence of magnetic stimuli on the meniscus shape of liquid bridge can be neglected here based on two facts. First, from Young's law,⁵³ the boundary of three phases (S/L/G) equilibrates depending on the inherent surface tension rather the external field stimuli. Second, we found no obvious changes in the meniscus of the MF bridge with various stimuli under the microscopic system (ESI,† Fig. S2).

Fig. 2c also shows a phenomenon that the capillary force of MF meniscus first decreased then increased with increasing d , giving a turning point around $d = 3$ mm. This is possibly due to the ΔH ($H_{\text{inside}} - H_{\text{boundary}}$) of the MF meniscus first increasing and then decreasing with increasing d (this can be directly reflected by the value of $H_{\text{center}} - H_{\text{boundary}}$ in Fig. 3c), which tuns the ΔP_{Mag} for capillary adhesion. Fig. 2d shows that capillary force decreased with the increased volume of MF meniscus. Actually, the increased volume of MF meniscus increased the L , *i.e.*, moved the boundary interface of MF–gas exterior, when under a mandatory indentation of probe. In such a case, the ΔH increased with the decrease in H_{boundary} .

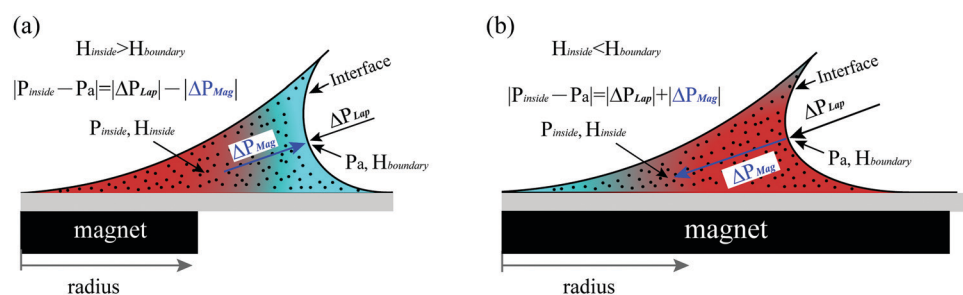


Fig. 4 Illustrating the mechanism of external magnetic field stimulating MF meniscus for switched capillary adhesion (red region signifying high field intensities and blue region signifying low ones). Application of the stimuli of coin-shaped magnet with (a) a small head face ($H_{\text{inside}} > H_{\text{boundary}}$) and (b) a large head face ($H_{\text{inside}} < H_{\text{boundary}}$). $|P_{\text{inside}} - P_{\text{a}}|$ reflecting the adhesion strength; ΔP_{Mag} caused by magnetic stimuli; ΔP_{Lap} caused by Laplace pressure.

Therefore, regardless of positive or negative, the value of ΔP_{Mag} will increase to weaken the contribution of $|P_{\text{inside}} - P_a|$ for the capillary adhesion of the MF meniscus. In general, the mechanisms of the magnetic field-regulated capillary adhesion of the MF meniscus have been revealed well in this paper. Briefly, if someone wants to weaken the capillary force of the MF meniscus, they should increase the magnetic field intensity inside the meniscus and decrease the magnetic field intensity of the boundary interface of the MF and gas, namely creating a large positive ΔP_{Mag} . If an enhanced capillary force is desired, the opposite can be performed for a large negative ΔP_{Mag} .

3.4 Theoretical adhesion models of MF meniscus under magnetic stimuli

For conveniently designing the magnetic stimuli for a controllable adhesive, the theoretical adhesion model of stimulated MF meniscus was built and solved for comparison to experimental results. Fig. 5a shows the physical model of the MF meniscus between the spherical probe and the glass substrate. The force of capillary adhesion $F_{\text{capillary}}$ is a result of the pressure difference $P_i - P_a$ between the probe surface OA P_i and the outer interface of liquid-gas BA P_a , *i.e.*, the atmosphere, and the surface tension force of meniscus F_{SF} . Based on the above discussion, the $P_i - P_a$ of the MF meniscus with magnetic stimuli is characterized by two factors: the Laplace pressure

$\Delta P_{\text{capillary}}$ and the magnetically induced pressure ΔP_{Mag} . Referring previous studies,^{50–52} Bernoulli equation of i and j point in MF meniscus under a magnetic field at a flow velocity of 0 is given by

$$P_i - \mu_0 \int_0^{H_i} M dH = P_j - \mu_0 \int_0^{H_j} M dH, \quad (1)$$

where P_i is the pressure at the point of i , H_i is the field intensity at point i , μ_0 is the magnetic permeability of free space, P_j is the pressure at point j (inner interface of MF-gas), H_j is the field intensity at the point of j , M is the magnetization of the MF, which can be regarded as a constant of the saturation magnetization of MF M_s when the intensity of stimulated field is much larger than the saturation magnetization of MF.⁵² Here, we neglect the influence of gravity and assume that the MF moves parallel to the substrate as the probe starts to detach. The boundary condition at j in the boundary interface of MF-gas can be written as⁵⁴

$$P_j + \frac{1}{2}\mu_0 M_n^2 = P_a + \Delta P_{\text{Lap}}, \quad (2)$$

where M_n is the normal component of M at the meniscus surface. After inserting eqn (2) and simplifying, eqn (1) leads to

$$P_i - P_a = \Delta P_{\text{Lap}} + \mu_0 M_s (H_i - H_j) - \frac{1}{2}\mu_0 M_n^2, \quad (3)$$

The total force of capillary adhesion of MF meniscus is a combination of the pressure difference $P_i - P_a$ acting upon a

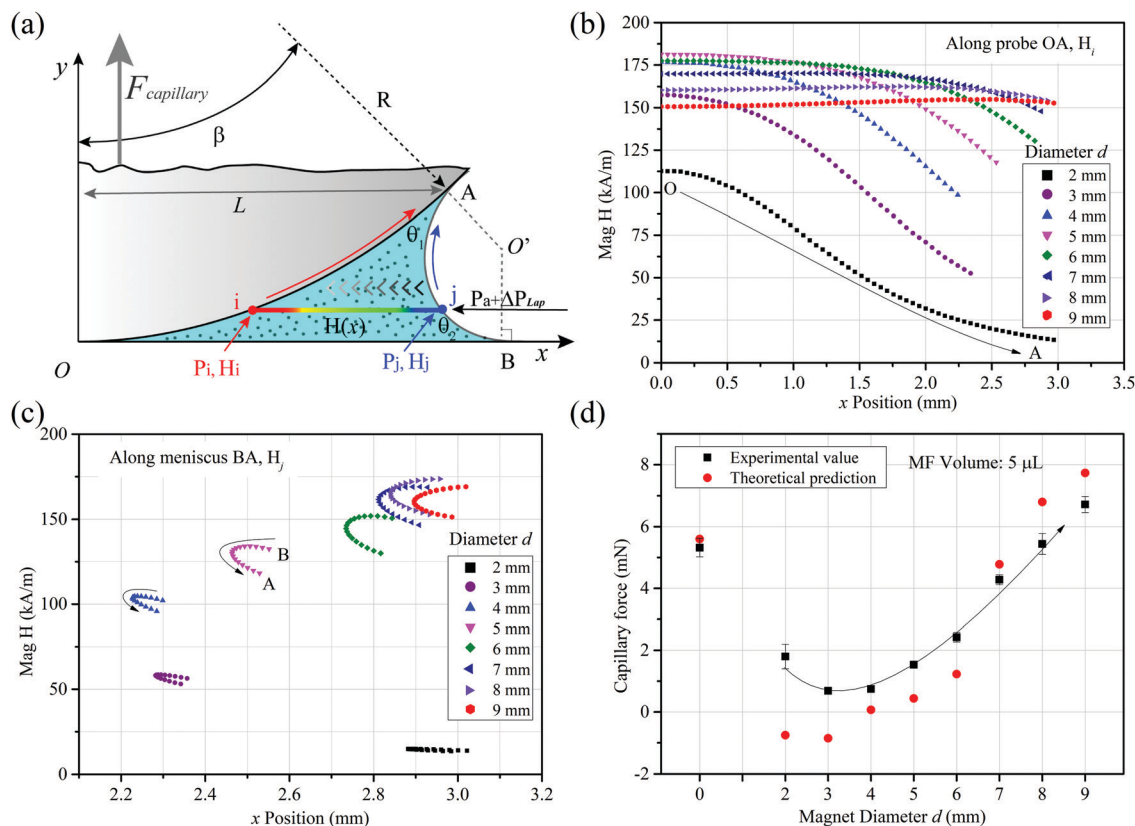


Fig. 5 (a) Physical model of the MF meniscus between the spherical probe and the glass substrate. Magnetic field intensity of (b) probe surface OA (H_i) and (c) meniscus interface BA (H_j) with different d as a function of position x on the substrate. (d) Theoretical results of magnetically stimulated capillary adhesion force with varying d in comparison to the experimental values.

cross-sectional area πL^2 and the surface tension force F_{SF} acting on interface of the meniscus. Thus, F_{adhesion} can be described as

$$F_{\text{capillary}} = \int_0^L (P_i - P_a) d(\pi x^2) + F_{\text{SF}}$$

$$= \pi L^2 \Delta P_{\text{Lap}} + F_{\text{SF}} + \int_0^L \left[\mu_0 M_s (H_i - H_j) - \frac{1}{2} \mu_0 M_n^2 \right] d(\pi x^2). \quad (4)$$

Based on a previous study,³² the original capillary force F of meniscus at constant liquid volume is given by

$$F = \pi L^2 \Delta P_{\text{capillary}} + F_{\text{SF}}$$

$$= -4\pi\gamma R \frac{\cos(\theta_1 + \beta) + \cos\theta_2}{2}, \quad (5)$$

where γ is the surface tension of the MF, R is the curve radius of probe, β is the filling angle, θ_1 and θ_2 are the contact angles of MF on the probe and substrate (see Fig. 5a). Replacing the original capillary force in eqn (4) and discretizing the integral part finally gives an explicit expression for the capillary adhesion of the MF meniscus at constant volume with magnetic-field stimuli:

$$F_{\text{capillary}} = -4\pi\gamma R \frac{\cos(\theta_1 + \beta) + \cos\theta_2}{2}$$

$$+ \sum_{k=1}^N \left[\mu_0 M_s (H_i(k) - H_j(k)) - \frac{1}{2} M_n(k)^2 \right] \frac{2k\pi L^2}{N^2}. \quad (6)$$

Thus, eqn (6) can be solved by the acquisition of $H_i(k)$ along the probe surface OA and of $H_j(k)$ and $M(k)$ along the meniscus surface BA. In this paper, the data of $H_i(k)$ and $H_j(k)$ for various diameters of magnets were accurately extracted from the simulation results (ESI,† Fig. S3) depending on their L and β (Fig. 2b), as shown in Fig. 5b and c. $M_n(k)$ is very difficult to acquire; for ease of calculation, it was approximately equated to M , *i.e.*, the constant M_s , because in practice, the field of the magnet diverges through the small meniscus with a large normal component. The parameters R , γ , M_s , L , and β are given in experimental section and Fig. 2c, and the measured contact angles of θ_1 and θ_2 are nearly zero (ESI,† Fig. S4). The detail process for calculation is schematically illustrated Fig. S5 in ESI.† Fig. 5c shows a graph of the calculated adhesion force of the MF meniscus (fixed at 5 μL) with the magnetic stimuli of varying d in comparison to the experimental results. It appears that our theoretical model performs well in the prediction of capillary adhesion force of the MF meniscus stimulated by a certain magnetic field.

4. Conclusion

We demonstrated the reversible wet-adhesion performance of MF meniscus between two surfaces under the external stimulus of a magnetic field. With the varying diameter of applied magnets, the capillary adhesion force of the MF meniscus underwent significant modulations, first decreasing then

increasing, and showing a switching behavior for adhesion. The increased volume of the stimulated meniscus played a weakened role in the adhesion strength, whereas little influence was found on the original capillary adhesion (without stimuli). Compared with the original capillary interaction, the stimulated interaction can be increased or decreased directly depending on the distribution of the magnetic field intensity. The underlying mechanism was revealed to be the additional hydrostatic pressure induced by the intensity difference in the magnetic field between the interior of the meniscus and liquid–gas boundary interface imposing a tuning effect on the pressure inside the MF meniscus, which is usually only dominated by the Laplace pressure in typical capillary adhesion. Furthermore, the relative physical model was also built and solved in comparison to the experimental data. The results indicate that our theories effectively predict the stimulated capillary force of the MF meniscus. In general, we present a pioneering work of magnetically induced reversible capillary adhesives, which can be regarded as a guide for further study in developing new controllable wet-adhesive systems.

Conflicts of interest

There are no conflicts to declare.

Acknowledgements

This work was supported by the National Natural Science Foundation of China (NSFC) (grant no. 51675268 and 51875278), and M. L. would like to thank the China Scholarship Council (no. 201806830076) for funding.

References

- 1 K. Autumn, Y. A. Liang, S. T. Hsieh, W. Zesch, W. P. Chan, T. W. Kenny, R. Fearing and R. J. Full, Adhesive force of a single gecko foot-hair, *Nature*, 2000, **405**(6787), 681–685.
- 2 K. Autumn, Gecko adhesion: structure, function, and applications, *MRS Bull.*, 2007, **32**(06), 473–478.
- 3 B. Zhao, N. Pesika, H. Zeng, Z. Wei, Y. Chen, K. Autumn, K. Turner and J. Israelachvili, Role of Tilted Adhesion Fibrils (Setae) in the Adhesion and Locomotion of Gecko-like Systems, *J. Phys. Chem. B*, 2008, **113**(12), 3615–3621.
- 4 K. Autumn, M. Sitti, Y. A. Liang, A. M. Peattie, W. R. Hansen, S. Sponberg, T. W. Kenny, R. Fearing, J. N. Israelachvili and R. J. Full, Evidence for van der Waals adhesion in gecko setae, *Proc. Natl. Acad. Sci. U. S. A.*, 2002, **99**(19), 12252–12256.
- 5 S. Reddy, E. Arzt and A. del Campo, Bioinspired Surfaces with Switchable Adhesion, *Adv. Mater.*, 2007, **19**(22), 3833–3837.
- 6 J. Cui, D. M. Drotlef, I. Larraza, J. P. Fernandez-Blazquez, L. F. Boesel, C. Ohm, M. Mezger, R. Zentel and A. del Campo, Bioinspired actuated adhesive patterns of liquid crystalline elastomers, *Adv. Mater.*, 2012, **24**(34), 4601–4604.
- 7 M. Frensemeier, J. S. Kaiser, C. P. Frick, A. S. Schneider, E. Arzt, R. S. Fertig and E. Kroner, Temperature-Induced

- Switchable Adhesion using Nickel-Titanium-Polydimethylsiloxane Hybrid Surfaces, *Adv. Funct. Mater.*, 2015, **25**(20), 3013–3021.
- 8 D. M. Drotlef, P. Blumler and A. del Campo, Magnetically actuated patterns for bioinspired reversible adhesion (dry and wet), *Adv. Mater.*, 2014, **26**(5), 775–779.
- 9 F. K. A. Chiao, Fabrication and Patterning of Magnetic Polymer Micropillar Structures Using a Dry-Nanoparticle Embedding Technique, *J. Microelectromech. Sys.*, 2013, **22**(1), 131–139.
- 10 J. Purto, M. Frensemeier and E. Kroner, Switchable Adhesion in Vacuum Using Bio-Inspired Dry Adhesives, *ACS Appl. Mater. Interfaces*, 2015, **7**(43), 24127–24135.
- 11 Y. Wang, H. Tian, J. Shao, D. Sameoto, X. Li, L. Wang, H. Hu, Y. Ding and B. Lu, Switchable Dry Adhesion with Step-like Micropillars and Controllable Interfacial Contact, *ACS Appl. Mater. Interfaces*, 2016, **8**(15), 10029–10037.
- 12 P. Y. Isla and E. Kroner, A Novel Bioinspired Switchable Adhesive with Three Distinct Adhesive States, *Adv. Funct. Mater.*, 2015, **25**(16), 2444–2450.
- 13 G. Hanna and W. J. P. Barnes, Adhesion and detachment of the toe pads of tree frogs, *J. Exp. Biol.*, 1991, **155**(1), 103–125.
- 14 D. M. Green and J. Carson, The adhesion of treefrog toe-pads to glass: cryogenic examination of a capillary adhesion system, *J. Nat. Hist.*, 1988, **22**(1), 131–135.
- 15 W. J. P. Barnes, Functional morphology and design constraints of smooth adhesive pads, *MRS Bull.*, 2007, **32**(06), 479–485.
- 16 D. M. Drotlef, E. Appel, H. Peisker, K. Dening, A. del Campo, S. N. Gorb and W. J. P. Barnes, Morphological studies of the toe pads of the rock frog, *Stauroids parvus* (family: Ranidae) and their relevance to the development of new biomimetically inspired reversible adhesives, *Interface Focus*, 2014, **5**(1), 20140036.
- 17 W. Huang and X. L. Wang, Biomimetic design of elastomer surface pattern for friction control under wet conditions, *Bioinspiration Biomimetics*, 2013, **8**(4), 046001.
- 18 S. Wang, M. Li, W. Huang and X. Wang, Sticking/Climbing Ability and Morphology Studies of the Toe Pads of Chinese Fire Belly Newt, *J. Bionic. Eng.*, 2016, **13**(1), 115–123.
- 19 M. Li, W. Huang and X. Wang, Bioinspired, peg-studded hexagonal patterns for wetting and friction, *Biointerphases*, 2015, **10**(3), 031008.
- 20 W. Federle, W. J. P. Barnes, W. Baumgartner, P. Drechsler and J. M. Smith, Wet but not slippery: boundary friction in tree frog adhesive toe pads, *J. R. Soc., Interface*, 2006, **3**(10), 689–697.
- 21 W. J. Barnes, M. Baum, H. Peisker and S. N. Gorb, Comparative Cryo-SEM and AFM studies of hylid and rhacophorid tree frog toe pads, *J. Morphol.*, 2013, **274**(12), 1384–1396.
- 22 D. M. Drotlef, L. Stepien, M. Kappl, W. J. P. Barnes, H. J. Butt and A. del Campo, Insights into the Adhesive Mechanisms of Tree Frogs using Artificial Mimics, *Adv. Funct. Mater.*, 2013, **23**(9), 1137–1146.
- 23 Y. Zhao, Y. Wu, L. Wang, M. Zhang, X. Chen, M. Liu, J. Fan, J. Liu, F. Zhou and Z. Wang, Bio-inspired reversible underwater adhesive, *Nat. Commun.*, 2017, **8**(1), 2218.
- 24 M. Li, J. Xie, Q. Dai, W. Huang and X. Wang, Effect of wetting case and softness on adhesion of bioinspired micropatterned surfaces, *J. Mech. Behav. Biomed. Mater.*, 2018, **78**, 266–272.
- 25 M. Li, Q. Dai, W. Huang and X. Wang, Pillar versus dimple patterned surfaces for wettability and adhesion with varying scales, *J. R. Soc., Interface*, 2018, **15**(148), 20180681.
- 26 J. Iturri, L. Xue, M. Kappl, L. García-Fernández, W. J. P. Barnes, H. J. Butt and A. del Campo, Torrent Frog-Inspired Adhesives: Attachment to Flooded Surfaces, *Adv. Funct. Mater.*, 2015, **25**(10), 1499–1505.
- 27 W. J. P. Barnes, *Adhesion in Wet Environments: Frogs*, Springer, Netherlands, 2012, p. 70–83.
- 28 B. N. J. Persson, Wet adhesion with application to tree frog adhesive toe pads and tires, *J. Phys.: Condens. Matter*, 2007, **19**(37), 376110.
- 29 X. Zhang, X. Yi, S. I. U. Ahmed, M. Kosinskiy, Y. Liu and J. A. Schaefer, Dynamic Contact Model Based on Meniscus Adhesion For Wet Bio-Adhesive Pads: Simulation Experiments, *Tribol. Trans.*, 2010, **53**(2), 280–287.
- 30 C. D. Willett, M. J. Adams, S. A. Johnson and J. P. K. Seville, Capillary Bridges between Two Spherical Bodies, *Langmuir*, 2000, **16**(24), 9396–9405.
- 31 M. Farshchitabrizi, M. Kappl, Y. Cheng, J. Gutmann and H. Butt, On the Adhesion between Fine Particles and Nanocontacts: An Atomic Force Microscope Study, *Langmuir*, 2006, **22**(5), 2171.
- 32 H. J. Butt and M. Kappl, Normal capillary forces, *Adv. Colloid Interface Sci.*, 2009, **146**(1–2), 48–60.
- 33 N. M. And and J. N. Israelachvili, Nanoscale Mechanisms of Evaporation, Condensation and Nucleation in Confined Geometries, *J. Phys. Chem. B*, 2002, **106**(14), 3534–3537.
- 34 A. A. Feiler, J. Stiernstedt, K. Theander, P. Jenkins and M. W. Rutland, Effect of Capillary Condensation on Friction Force and Adhesion, *Langmuir*, 2007, **23**(2), 517.
- 35 M. M. Kohonen, N. Maeda and H. K. Christenson, Kinetics of Capillary Condensation in a Nanoscale Pore, *Phys. Rev. Lett.*, 1999, **82**(23), 4667–4670.
- 36 J. B. Sokoloff, Effects of Capillary Forces on a Hydrogel Sphere Pressed against a Surface, *Langmuir*, 2016, **32**(1), 135–139.
- 37 B. Bhushan, Adhesion and stiction: mechanisms, measurement techniques, and methods for reduction, *J. Vac. Sci. Technol., B: Microelectron. Nanometer Struct.–Process., Meas., Phenom.*, 2003, **21**(6), 2262–2296.
- 38 Y. E. Liang, Y. H. Weng, H. K. Tsao and Y. J. Sheng, Meniscus Shape and Wetting Competition of a Drop between a Cone and a Plane, *Langmuir*, 2016, **32**(33), 8543–8549.
- 39 L. Yang, Y.-s. Tu and H.-l. Tan, Influence of atomic force microscope (AFM) probe shape on adhesion force measured in humidity environment, *J. Appl. Math. Mech.*, 2014, **35**(5), 567–574.
- 40 S. H. Chen and A. K. Soh, The capillary force in micro- and nano-indentation with different indenter shapes, *Int. J. Solids Struct.*, 2008, **45**(10), 3122–3137.

- 41 E. J. D. Souza, M. Brinkmann, C. Mohrdieck and E. Arzt, Enhancement of Capillary Forces by Multiple Liquid Bridges, *Langmuir*, 2008, **24**(16), 8813–8820.
- 42 E. J. D. Souza, M. Brinkmann, C. Mohrdieck, A. Crosby and E. Arzt, Capillary Forces between Chemically Different Substrates, *Langmuir*, 2008, **24**(18), 10161–10168.
- 43 S. Cai and B. Bhushan, Meniscus and viscous forces during separation of hydrophilic and hydrophobic surfaces with liquid-mediated contacts, *Mater. Sci. Eng., R*, 2008, **61**(1-6), 78–106.
- 44 H. Yi, S. H. Lee, M. Seong, M. K. Kwak and H. E. Jeong, Bioinspired Reversible Hydrogel Adhesive for Wet and Underwater Surfaces, *J. Mater. Chem. B*, 2018, **6**(48), 8064–8070.
- 45 H. Chen, A. Amirfazli and T. Tang, Modeling liquid bridge between surfaces with contact angle hysteresis, *Langmuir*, 2013, **29**(10), 3310–3319.
- 46 F. Restagno, C. Poulard, C. Cohen, L. Vagharchakian and L. Leger, Contact angle and contact angle hysteresis measurements using the capillary bridge technique, *Langmuir*, 2009, **25**(18), 11188–11896.
- 47 E. J. De Souza, L. Gao, T. J. McCarthy, E. Arzt and A. J. Crosby, Effect of contact angle hysteresis on the measurement of capillary forces, *Langmuir*, 2008, **24**(4), 1391–1396.
- 48 M. Li, W. Huang and X. Wang, Advanced adhesion and friction measurement system, *Meas. Sci. Technol.*, 2017, **28**(3), 035601.
- 49 V. Bashtovoi, P. Kuzhir and A. Reks, Capillary ascension of magnetic fluids, *J. Magn. Magn. Mater.*, 2002, **252**(252), 265–267.
- 50 V. Bashtovoi, G. Bossis, P. Kuzhir and A. Reks, Magnetic field effect on capillary rise of magnetic fluids, *J. Magn. Magn. Mater.*, 2005, **289**, 376–378.
- 51 Z. Wang, Z. Hu, W. Huang and X. Wang, Elastic support of magnetic fluids bearing, *J. Phys. D: Appl. Phys.*, 2017, **50**(43), 435004.
- 52 S. G. E. Lampaert, J. W. Spronck and R. A. J. van Ostayen, Load and stiffness of a planar ferrofluid pocket bearing, *Proc. Inst. Mech. Eng., Part J*, 2017, **232**(1), 14–25.
- 53 P. G. D. Gennes, F. Brochard-Wyart and D. Quéré, *Capillarity and Wetting Phenomena*, Springer, New York, 2004, p. 1700.
- 54 S. Kamiyama and K. Koike, Hydrodynamics of magnetic fluids, *Braz. J. Phys.*, 1995, **25**(2), 83–100.